frontiers | Frontiers in Earth Science

TYPE Original Research
PUBLISHED 10 October 2023
DOI 10.3389/feart.2023.1251107

OPEN ACCESS

EDITED BY
Xijun Liu,
Guilin University of Technology, China

REVIEWED BY
Yaqi Yang,
Guizhou University, China
Zhang Zhiguo,
Hexi University, China
Fang An,
Northwest University, China

*CORRESPONDENCE
Yu-Li He,
heyuli301@126.com

RECEIVED 30 June 2023
ACCEPTED 22 September 2023
PUBLISHED 10 October 2023

CITATION
Wang W-J, He Y-L, Xu L, Xu W-B, Ren W-X and Wang H-T (2023), Chronology and geochemistry of Late Carboniferous volcanics in Bogda, Xinjiang: implications for the tectonic evolution of the Eastern Tianshan. *Front. Earth Sci.* 11:1251107. doi: 10.3389/feart.2023.1251107

Chronology and geochemistry of Late Carboniferous volcanics in Bogda, Xinjiang: implications for the tectonic evolution of the Eastern Tianshan

Wen-Jia Wang[1,2], Yu-Li He[3,4]*, Lei Xu[2], Wen-Bo Xu[5], Wen-Xiu Ren[2] and Huai-Tao Wang[2]

[1]School of Earth Sciences and Resources, China University of Geosciences, Beijing, China, [2]Geological Survey of Gansu Province, Lanzhou, China, [3]School of Geographical Sciences, China West Normal University, Nanchong, China, [4]Sichuan Provincial Engineering Laboratory of Monitoring and Control for Soil Erosion on Dry Valleys, China West Normal University, Nanchong, China, [5]Key Laboratory of Mineral Resources in Western China (Gansu Province), School of Earth Sciences, Lanzhou University, Lanzhou, China

The Late Carboniferous volcanic magmatic evolution in the Bogda Orogenic Belt is considerably important for understanding the evolution history of the Eastern Tianshan in the Central Asian Orogenic Belt. Our study focuses on the Upper Carboniferous Liushugou Formation in the Liudaogou and Qidaogou sections of Xishan Township in eastern Bogda. By analyzing the volcanics and sedimentary sequences, we present paleontological evidence, new zircon U–Pb ages, and geochemical data of the volcanics. The lithological composition of volcanics ranges from basic to acidic. The rhyolite has an age of 311.2 ± 1.7 Ma, which, when combined with guide fossils *Plerophyllum* sp., *Zaphrentoides* sp., and *Zaphrentites* sp., indicates its formation in the Late Carboniferous. The geochemical and zircon Lu–Hf isotopic data (εHf(t) = 8.0–11.9) indicate that the basalts originated from a metasomatized subcontinental lithospheric mantle, while andesites and rhyolites were products of crystallization differentiation of the basalts that underwent assimilative mixing. Based on the published data, we propose that the tectonic evolution, transitioning from island arc magmatic systems to post-collisional orogenic belts, commenced in the Bogda Orogenic Belt toward the end of the Late Carboniferous.

KEYWORDS

Late Carboniferous, volcanics, tectonic transition, Bogda Orogenic Belt, Eastern Tianshan

1 Introduction

The Central Asian Orogenic Belt (CAOB) is a colossal and formed Phanerozoic accretionary orogenic belt (Sengör et al., 1993; Windley et al., 2007; Kröner et al., 2014; Xiao et al., 2018) comprising various accretionary complexes, ophiolite mélange belts, magmatic arcs, arc-related basins, continental fragments and seamounts (Charvet et al., 2007; Han et al., 2010; Xiao et al., 2010; Shu et al., 2011; Glorie et al., 2011; Long et al., 2012; Ao et al., 2016; Yang et al., 2020; Yang et al., 2021; Mao et al., 2022; Wang et al., 2023). The China Tianshan Belt is located at the southernmost part of the CAOB (Figure 1A; Xiao et al., 2004a; Wang et al., 2007), and it spans over 2,500 km from west–east, and is an important

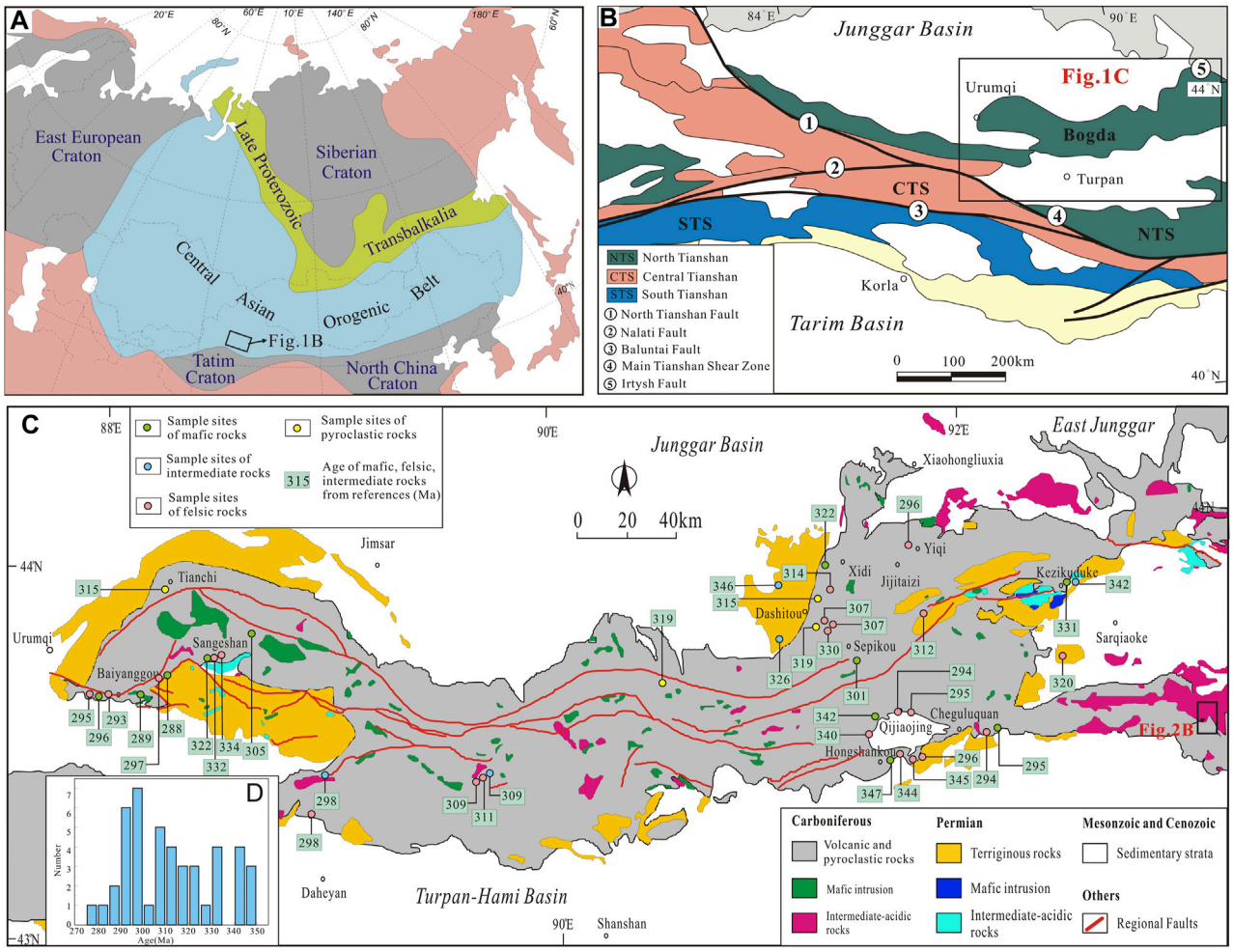

FIGURE 1
(A) Geological map of the CAOB (modified after Jahn et al., 2000); **(B)** Geological map of the Tianshan Belt (modified after Wang et al., 2011); **(C)** Simplified tectonic map of the BOB (after Chen et al., 2011); **(D)** Histogram showing zircon U–Pb ages of Carboniferous to Permian volcanics. Detailed data are presented in Supplementary Table S1.

research area for understanding the tectonic evolution of the CAOB in the Paleozoic (Xiao et al., 2004a; Wang et al., 2007; Sun et al., 2008). The Tianshan Belt can be geographically divided into the western and eastern segments, with a boundary that runs roughly along the Urumqi–Korla road. The Eastern Tianshan Belt is tectonically divided into three parts: South, Middle, and North Tianshan (Figure 1B). The Bogda Orogenic Belt (BOB) belongs to the Eastern Tianshan segment, which serves as an important information source for understanding the Paleo-Asian Ocean subduction–accretion geodynamic evolution in the CAOB (Shu et al., 2011; Liu et al., 2020).

The bimodal volcanic suite refers to a collection of rock assemblages predominantly composed of basaltic and acidic rocks (Pin and Paquette, 1997; Shinjo and Kato, 2000). These rocks are commonly found in extensional settings and associated with within-plate, post-collisional, or back-arc rifting settings (Zhang et al., 2008). Their discovery provides direct evidence for crust–mantle interaction (Aydin et al., 2014). However, the lack of intermediate rocks within this suite has always been a topic of discussion. One theory suggests that, although intermediate magma may have existed, it failed to reach the surface for various reasons. Another explanation proposes that intermediate rocks may have resulted from the mixing of basaltic and rhyolitic magma, leading to their relative scarcity (Peccerillo et al., 2003; Aydin et al., 2014; Zhang et al., 2020).

The Late Paleozoic bimodal volcanics are abundant in the BOB (Figure 1C; Zhang et al., 2017); however, their origin continued to be a subject of controversy, with different hypotheses, including continental rifting, island arcs, post-collisional environments, and mantle plume-related Large Igneous Provinces (LIPs) (Xia et al., 2004; Xia et al., 2012; Wali et al., 2018). The connection between the felsic and basaltic volcanics continues to be unclear, hampering our comprehension of their genesis and associated geodynamic mechanisms.

We have undertaken field investigations and stratigraphic, paleontological, chronological, and geochemical studies of volcanic and sedimentary sequences during the Carboniferous to Permian period in eastern BOB. On these investigation, we generated previously published data of the BOB to investigate the petrogenesis and diagenetic relationships of intermediate rocks in

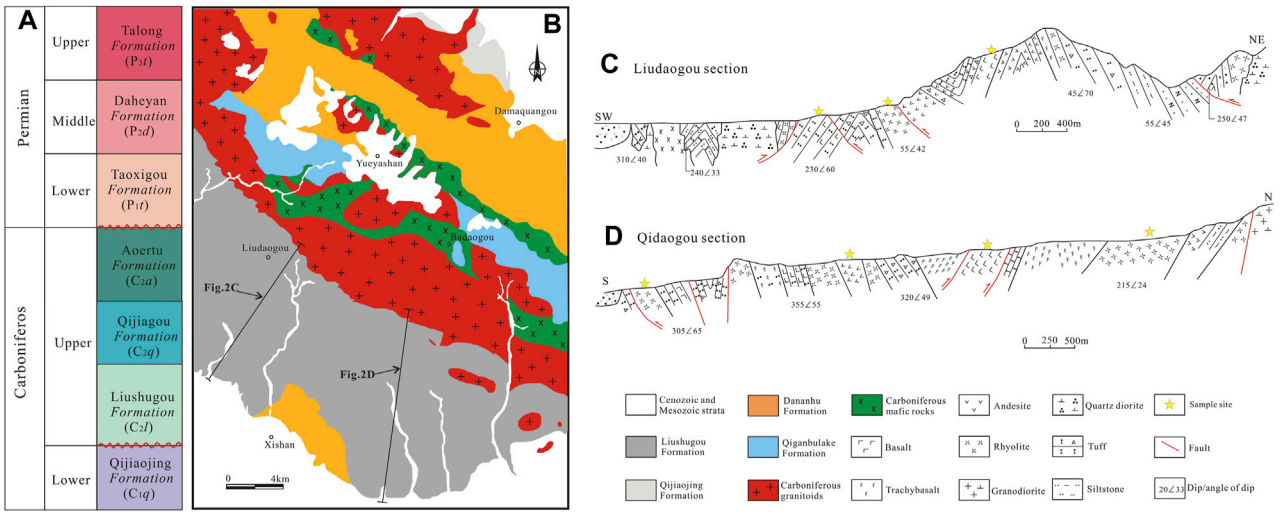

FIGURE 2
(A) Simplified stratigraphy column of the Late Paleozoic in the BOB (after He et al., 1994); **(B)** Geological map of the Xishan area in the eastern BOB; geological sections showing volcanics sampling sites; **(C)** Liudaogou section and **(D)** Qidaogou sections.

the bimodal volcanic suites as well as the geodynamic processes that have contributed to the Carboniferous to Permian evolution in the Eastern Tianshan.

2 Geological setting

The BOB, which spans approximately 600 km, separates the Junggar and the Turpan–Hami Basins in northern China (Figure 1C). It extends from Urumqi in the west to the Hongliuxia–Suji area in the east, where it connects with the Kelameili Orogenic Belt. The BOB was formed during the Devonian to Carboniferous period as an island arc due to the subduction of the Kelameili ocean (Xiao et al., 2004a). The Carboniferous strata with 4,500 m thickness are exposed in the BOB (Wartes et al., 2002), as shown in Figure 2A. The Lower Carboniferous is primarily comprised of tuffaceous sandstones, marine volcanic tuffs, and volcanic lavas (Wali et al., 2018). In contrast, the Upper Carboniferous primarily consists of shallow marine limestones, sandstones, and mudstones, often accompanied by submarine basalts, andesites, rhyolites, and felsic tuffs (Chen et al., 2011). The Permian strata are sporadically scattered across the BOB, and the specific stratigraphic composition is shown in Figure 2. The Lower Permian stratigraphy contains conglomerates, sandstones, and mudstones, reflecting an alluvial fan environment. In addition, multiple volcanic rock layers are present within these sequences. The Middle Permian, comprising mudstones, siltstones, and conglomerates, is considered evidence of a shallow lake plain environment. The thick red conglomerates of the Upper Permian indicate the presence of a terrestrial environment (Wartes et al., 2002). The study area belongs to Hami in the southern Junggar and is the easternmost section of the BOB. It is dominated by the Devonian to Carboniferous strata and Carboniferous intrusive rocks (Figure 2B). The Dananhu Formation is mainly composed of tuffs, basalts, bioclastic tuffs, and slates. The Qijiaojing Formation mainly comprises rhyolites and basalts interbeds with tuffaceous sandstones (Gu et al., 2000). The Liushugou Formation mainly consists of basalts, basaltic andesites, rhyolites, and other bimodal volcanics (Zhang et al., 2017).

3 Sampling and petrography

In this field survey, we have chosen two stratigraphic sections located in Xishan Township, the Liudaogou and Qidaogou sections (Figures 2C, D). Both sections are approximately 4,000 m thick and belong to the Upper Carboniferous Liushugou Formation (C_2l). The Liushugou Formation is in fault contact with the Early Carboniferous granodiorite pluton to the north. Meanwhile, the southern part is predominantly covered with Quaternary sediments and in an angular unconformity contact with the underlying Dananhu Formation (D_1d). The Liushugou Formation is mainly composed of four sections. The first section is characterized by intermediate-acid volcanics and volcanic lava containing rhyolite, tuff, and siltstone, among which is produced the fossil *Bellerophonids*. The second section is characterized by intermediate-acid volcanics intercalated with intermediate-basic volcanics and volcanic lava. It is mainly composed of andesite, rhyolitic andesite, and basalt. The third section is characterized by volcanics intercalated with sedimentary rocks. It mainly comprises grayish white rhyolitic tuffs, andesites, gray fine sandstones, purplish red muddy siltstones, and bioclastic limestone. The fossils collected from the bioclastic limestone were *Plerophyllum* sp., *Zaphrentoides* sp., and *Zaphrentites* sp. Finally, the fourth section is characterized by acidic volcanic lava intercalated with the amount of intermediate-basic volcanics, including rhyolite, dacite, and basalt.

Basalt with dark grayish-green (Figure 3A) is characterized by vesicularity and intergranular textures and contains plagioclase (~72%), pyroxene (~25%), and greenite and calcite (~3%). The plagioclase (0.15–1 mm) is hypidiomorphic and broad tabular in

FIGURE 3
Representative field photos and photomicrographs. **(A, D)** Basalts, **(D)** showing a typical intergranular texture; **(B, E)** andesites, showing a typical porphyritic texture; **(C, F)** rhyolites, showing a typical porphyritic texture and rhyolitic structure. **(D–F)** The photomicrographs under cross-polarised light. Mineral abbreviations: Cpx-clinopyroxene; Pl-plagioclase; Qz-quartz.

shape, while the pyroxene (0.15–2 mm) is predominantly xenomorphic granular (<1 mm) (Figure 3D). Andesite with dark purple-red (Figure 3B) is primarily composed of matrix and phenocrysts. The phenocrysts are predominantly composed of plagioclase (~15%), while the matrix mostly consists of microcrystalline plagioclase (~75%). The plagioclase phenocrysts exhibit hypidiomorphic crystal and stout prismatic shapes with a small amount of kaolinization and sericitization plagioclase. Fine apatite and visible zircon (~0.5 mm) can also be found (Figure 3E). Rhyolite with a dark violet-red (Figure 3C) is characterized by porphyritic texture and rhyolitic structure, and its phenocrysts primarily comprise plagioclase (~10%) and quartz (~15%), while the matrix (~70%) with serious alteration is mostly cryptocrystalline (Figure 3F). The plagioclase phenocrysts (0.13–1.55 mm) display hypidiomorphic crystal and stout prismatic shapes with a small amount of kaolinization and sericitization (Figure 3F).

Six representative volcanic rock samples (i.e., two basalts, two andesites, and two rhyolites) in the Liudaogou section were selected for the whole-rock geochemical analysis. Eight representative volcanic rock samples (i.e., two basalts, two andesites, and four rhyolites) in the Qidaogou section were chosen for the geochemical analysis. Finally, a rhyolite sample was used for the zircon U–Pb dating.

4 Analytical methods

Zircon selection was performed by Langfang Chenshuo Rock and Mine Inspection Technology Service, Co. (Langfang, China). Cathodoluminescence images, U–Pb dating and trace element analysis of zircon were obtained from the Wuhan Sample Solution Analytical Technology Co., Ltd. (Wuhan, China). The U–Pb dating and trace element analysis were carried out via LA–ICP–MS. The detailed experimental process and operating conditions of the data processing methods were established by following a previous report by Zong et al. (2017). Zircon standard GJ-1 provided the weighted average U–Pb ages of 601.8 ± 2.5 Ma (n = 20), which closely corresponded with that in the previous studies ($^{206}Pb/^{238}U$ = 599.8 ± 4.5 Ma, Jackson et al., 2004).

The *in-situ* Hf isotope ratio analysis experiment was conducted using MC–ICP–MS in the same lab (Wuhan, China). The replicate analyses of GJ-1, 91,550, and Plešovice zircon standards during the analytical session produced mean $^{176}Hf/^{177}Hf$ ratios of 0.282001 ± 0.000012 (n = 4), 0.282286 ± 0.000012 (n = 4), and 0.2824779 ± 0.0000076 (n = 8), respectively, in good agreement with the previously published values (Zhang et al., 2020).

Fresh rock samples are to be ground to 200 mesh using a vibratory disk mill for elemental analyses. The major elements in these rock samples were analyzed using XRF (PANalytical Axios) at the Hubei Geological Research Laboratory. Based on the measured values of Chinese national rock standards (i.e., GSR-1 and GSR-2), the analytical accuracy obtained for all major oxides has been generally better than 2%. The trace element analyses were completed using ICP–MS (Thermo X Series II). The analysis accuracy was mostly usually better than 5%.

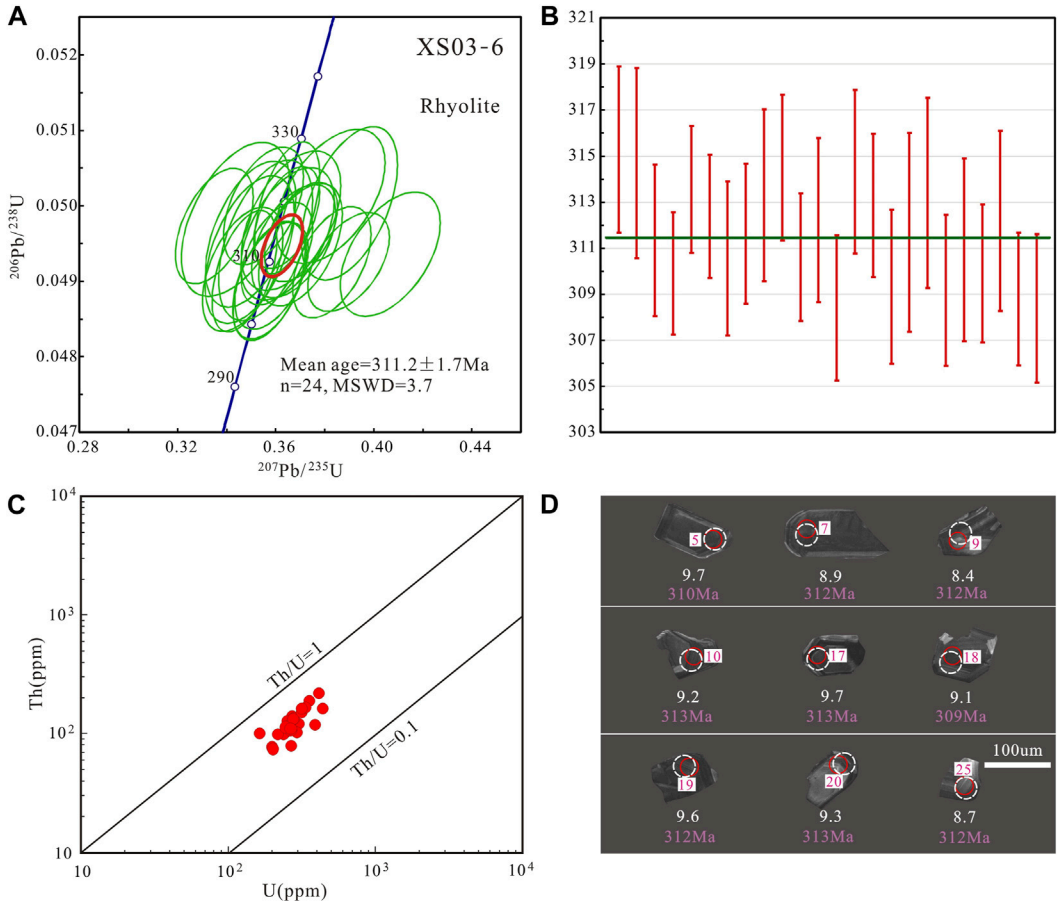

FIGURE 4
(A) and **(B)**: Zircon U–Pb concordia and weighted mean $^{206}Pb/^{238}U$ age diagrams for rhyolite (sample No. XS03-6), respectively; **(C)** Th vs. U diagram; **(D)** The representative cathodoluminescence images of the analyzed zircons. Red circles represent the spot of analysis for U–Pb dating. White circles represent the spot of analysis for Hf isotope.

5 Analytical results

Supplementary Table S2 presents the zircon U–Pb isotope analysis data of the Qidaogou rhyolite sample, XS03-6. Supplementary Tables S3, 4 list the whole-rock major and trace elements and Hf isotope analysis results.

5.1 Chronology

Zircons from the Qidaogou rhyolite sample are transparent, short columnar to prismatic, and have distinct rhythmic zoning, indicating that they belong to magmatic zircons. Their size is in the range of 40–120 μm, and length to width ratio is between 1:1 to 2:1 (Figure 4). Figure 4C shows that they have variable U (163–439 ppm) and Th (75–222 ppm) contents, with Th/U ranging from 0.30 to 0.62, indicating their magmatic origins (Harley and Kelly, 2007). Twenty-two zircon grains from the XS03-6 yielded a weighted mean $^{206}Pb/^{238}U$ age of 311.2 ± 1.7 Ma (Figure 4A), which is considered as the extrusive age of Qidaogou rhyolites.

Guide fossils are valuable tools for determining the stratigraphy age and understanding the living environment of organisms in a given period. They are commonly used as marks for regional stratigraphic comparisons (Peppe and Deino, 2013). In our recent field survey, we collected 15 fossil samples from the biological limestone of the Liudaogou and Qidaogou sections of the Liushugou Formation (C_2l^3). Accordingly, we identified three fossil groups, namely, *Plerophyllum* sp., *Zaphrentoides* sp., and *Zaphrentites* sp., which are all Carboniferous guide fossils (Figure 5). These were consistent with the age of our rhyolite.

5.2 Major and trace element geochemistry

We selected 14 representative samples from the studied region for the whole-rock major and trace element analyses. Supplementary Table S3 presents the results. The major element contents were standardized to 100% (volatile-free) before plotting the discrimination diagrams. The volcanics were divided into three groups according to their geochronology and geochemical features: basalts, andesites, and rhyolites (Figure 6).

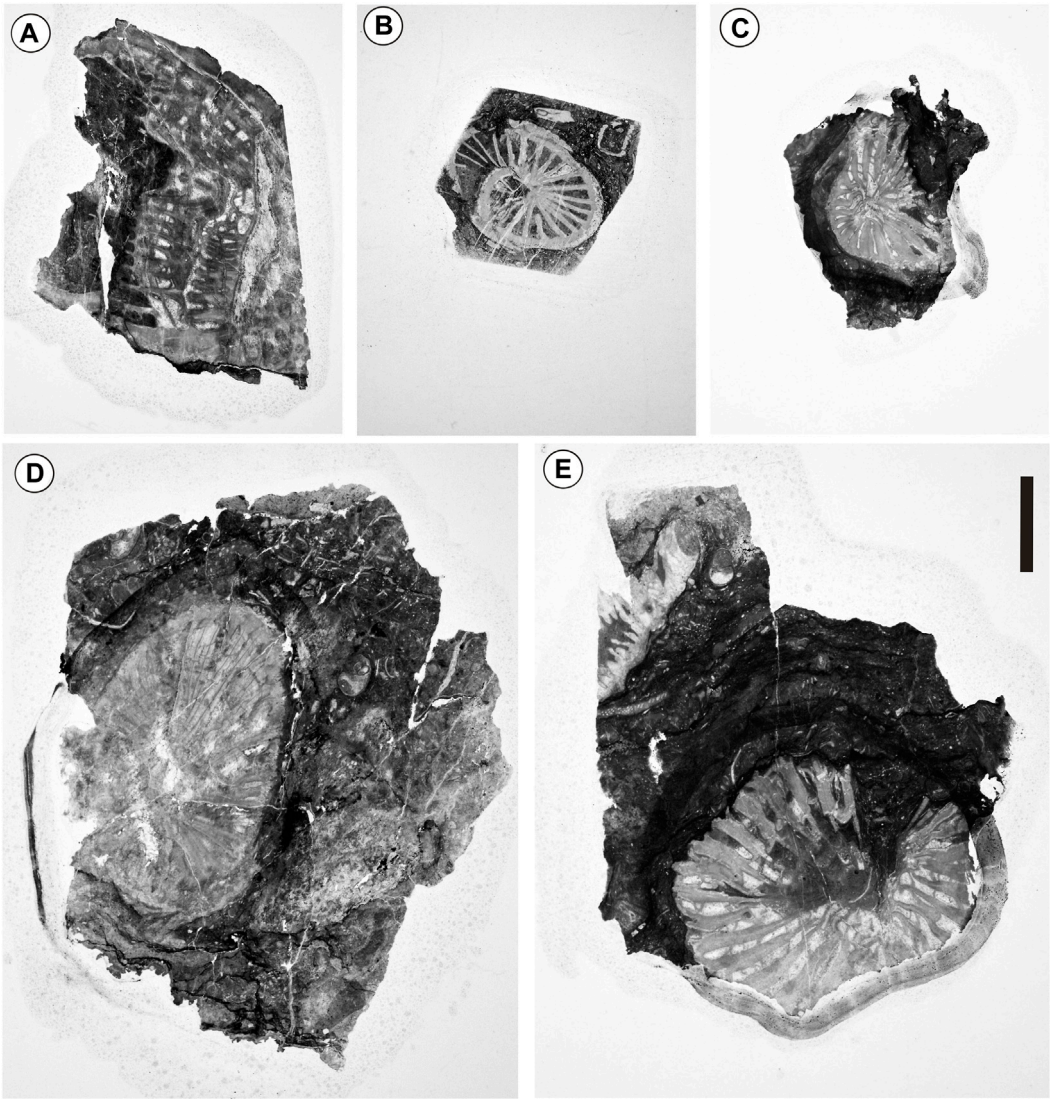

FIGURE 5
Coral fossils from the biological limestone of the Liushugou Formation. **(A, D)** *Zaphrentoides* sp.; **(B)** *Zaphrentites* sp.; **(C, E)** *Plerophyllum* sp. Scale bar = 1 cm. Fossil identification work was completed by the Nanjing Institute of Geology and Paleontology, Chinese Academy of Sciences.

Basalts have similar geochemical compositions, such as low SiO_2 (47.05–54.72 wt%) (volatile-free) and total alkali contents (4.82–5.37 wt%), but they have relatively high MgO (5.66–6.48 wt %), total Fe_2O_3 (8.38–13.46 wt%), Al_2O_3 (15.59–17.83 wt%), and TiO_2 (1.53–3.52 wt%) contents. Four andesite samples were characterized by medium SiO_2 (55.79–62.77 wt%), Mg# (44–55) and total alkali contents (5.15–7.30 wt%) and high Al_2O_3 (14.32–17.09 wt%) and CaO (5.04–8.78 wt%) contents. By contrast, the rhyolite samples had comparatively high SiO_2 (65.95–76.07 wt%) and total alkali contents (7.57–9.26 wt%) and low CaO (0.43–3.46 wt%), MgO (0.18–1.37 wt%), and total Fe_2O_3 (1.75–4.63 wt%) contents (Supplementary Table S2). Most of the volcanics were plotted in the calc-alkaline series in the TAS and AFM diagrams (Figures 6A, B) and as metaluminous in Figure 6C. All samples showed roughly similar rare-earth elements (REEs) and chondrite-normalized patterns. Compared with heavy REEs (HREEs), light REEs (LREEs) is considerably enriched with REEs (Figures 7A–C). The basalt samples yielded comparatively lower $(La/Yb)_N$ ratio (3.53–5.22) and LREE/HREE ratio (4.15–5.08) than the andesite and rhyolite samples with $(La/Yb)_N$ ratio (4.48–7.53) and LREE/HREE ratio (5.31–7.53), respectively (Supplementary Table S2). In Figure 7, the basalts and andesites showed relative enrichment of large ion lithophile elements (LILEs) (e.g., Rb, Ba, and Sr) and a depletion of high field strength elements (HFSEs) (Figures 7D, E). Meanwhile, the rhyolite samples were rich in the LILEs but lacking HFSEs (Figure 7F). The negative Eu anomalies (δEu = 0.58–0.86) along with Sr depletion indicate feldspar fractionation.

5.3 Zircon Lu–Hf isotope analysis

Fifteen zircon grains from the rhyolite (Sample No. XS03-6) were selected for the Hf isotope analysis. Supplementary Table S4 provides analytical data showing low $^{176}Lu/^{177}Hf$ ratios (<0.003164);

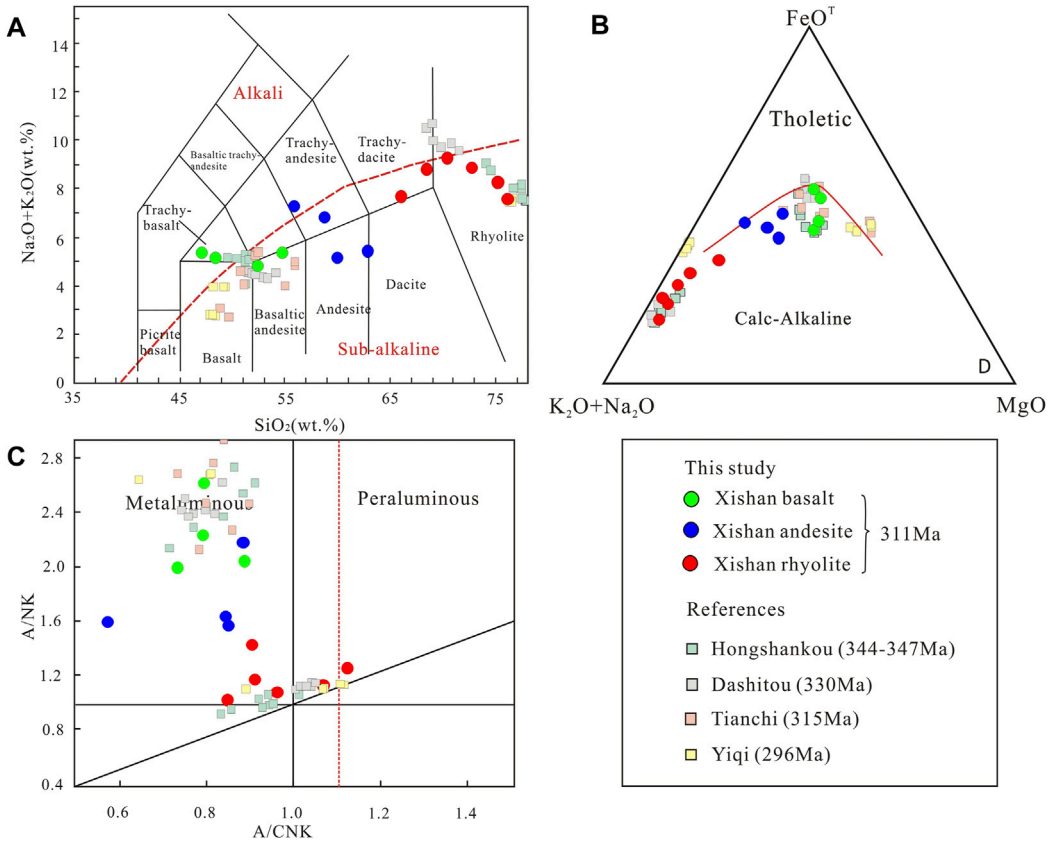

FIGURE 6
(A) TAS diagram (after Middlemost, 1994). **(B)** AFM diagram (after Irvine and Baragar, 1971). **(C)** A/NK vs. A/CNK (after Maniar and Piccoli, 1989). The data for the Hongshankou are adopted from Chen et al. (2013). The data for the Dashitou are adopted from Zhang et al. (2017). The data for the Tianchi are adopted from Xie et al. (2016) and that for the Yiqi are from Wang et al. (2010).

however, the tested $^{176}Hf/^{177}Hf$ ratios widely varied from 0.282823 to 0.282931. The calculated εHf(t) values were all positive and ranged from 8.0 to 11.9 (Figure 8; Supplementary Table S4). The T_{DM2} (Hf) model ages were also relatively low and ranged from 817 to 566 Ma.

6 Discussion

6.1 Spatial and temporal distributions of volcanics in the BOB

The BOB is a geologically intricate formation running from east to west and is widely acknowledged as one of the foremost volcanic belts in the Eastern Tianshan region during the Late Paleozoic. Distinguished by the extensive eruption of bimodal volcanics during the Carboniferous–Early Permian period, the belt has been subjected to detailed chronological studies (Figure 1C; Supplementary Table S1).

The chief geological components of the BOB include Carboniferous volcanics with basalt, andesite, rhyolite, tuff, and dacite formations as the dominant lithological assemblages, along with some intrusive rocks from the Carboniferous and Permian periods. The Bogda age histogram (Figures 1C, D) shows that volcanic activities have three clearly noticeable regularities: Early Carboniferous (345–330 Ma) distributed in the Sangeshan–Hongshankou–Kezikuduke area (Wang et al., 2006; Tan et al., 2010; Chen et al., 2013); Late Carboniferous (320–305 Ma) distributed in the Dashitou–Sepigou–Ertangou area (Gao et al., 2014; Wang et al., 2015b; Xie et al., 2016); and Early Permian (298–288 Ma) distributed in the Baiyanggou–Yiqi–Cheguluquan area (Wang et al., 2010; Shu et al., 2011; Chen et al., 2011; Chen et al., 2013). The new zircon age from this study indicated that the volcanic activity of the Xishan Liushugou Formation occurred during the Late Carboniferous (311.2 ± 1.7 Ma) and represented a multiple-stage eruption of the volcanics in the BOB, which may have been continuous from the Carboniferous to the Early Permian. Previous authors presented some controversial tectonic backgrounds of the Carboniferous and Permian volcanics in the BOB; therefore, further discussion is required.

6.2 Petrogenesis

6.2.1 Petrogenesis of the basalts

The basalts under investigation had low SiO_2, MgO, and Fe_2O_3 but showed relatively high enrichment in the Cr content, suggesting that their magma source region originated from the mantle (Zhang et al., 2017). Whereas the Ni (31–47 ppm) and Cr (41–143 ppm)

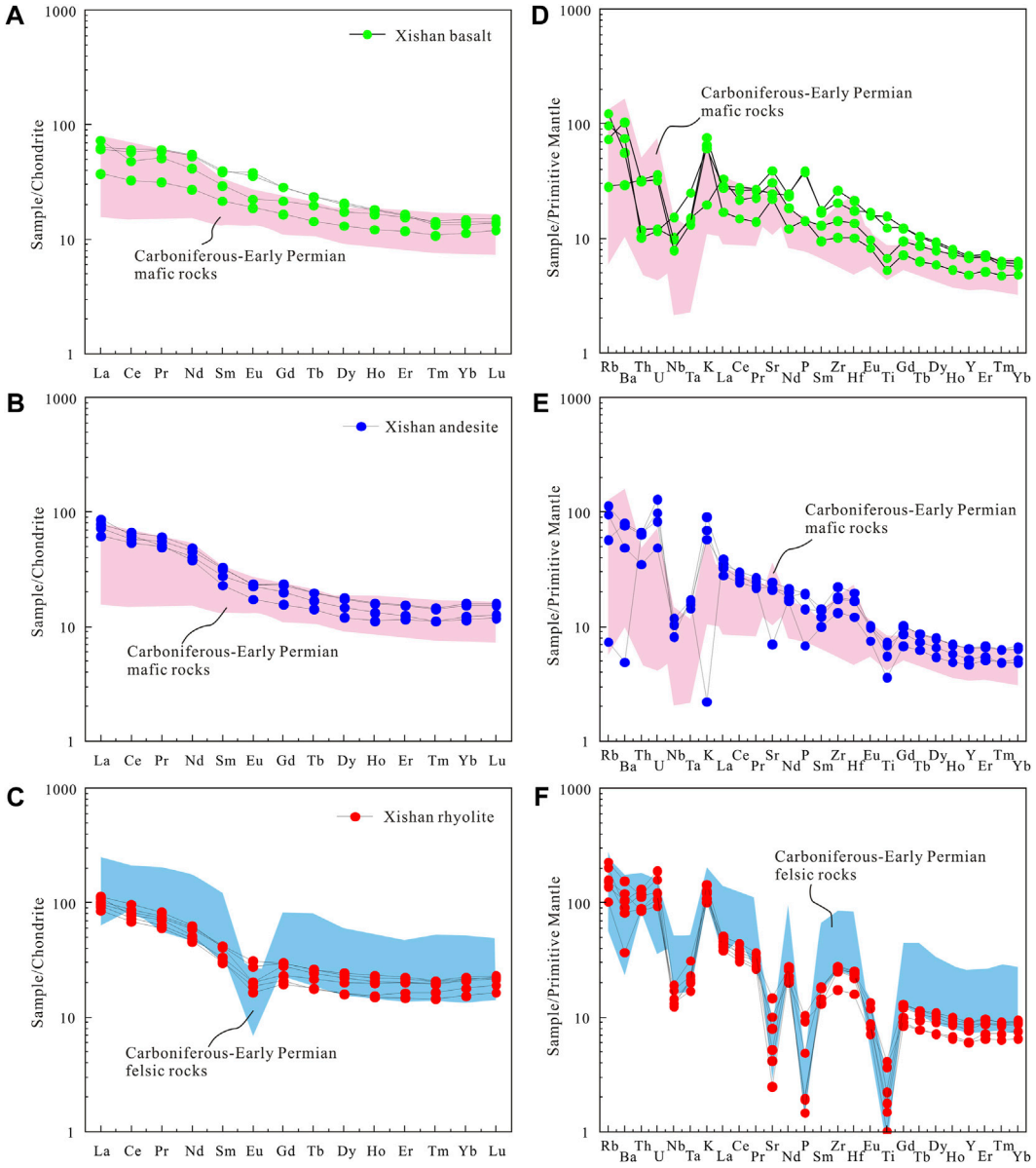

FIGURE 7
Chondrite-normalized REE patterns **(A–C)** and N-MORB normalized trace element spider diagrams **(D–F)** for volcanics in the eastern BOB. The values of chondrite and N-MORB are adopted from Sun and McDonough (1989). Data sources are the same as in Figure 6.

contents were remarkably lower than those of primary mantle-derived magmas (e.g., Ni = 300–400 ppm, Cr = 300–500 ppm; Frey et al., 1978), suggesting that they did not represent primary magmas and underwent obvious crystallization fractionation. The inverse relation among MgO, TFe_2O_3, CaO/Al_2O_3, CaO, and SiO_2 (Figure 9) indicated that they were likely formed through pyroxene and olivine fractionation. However, the positive anomalies of Eu and Sr (Figure 7) implied that the plagioclase fractionation was insignificant.

All of the basalt samples collected in the study area exhibited considerable Nb–Ta anomalies (Figure 7). Moreover, their Nb/La, Ce/Pb, and Nb/Yb ratios were significantly different from those of oceanic island basalt (OIB) (Hofmann, 1997). Two possible causes for this are as follows. One was derived from an arc-related tectonic environment, while the other was produced in a within-plate tectonic background and underwent crustal contamination or originated from a metasomatized subcontinental lithospheric mantle (SCLM). The variation charts (Figures 10A, B) showed the MORB trend to the SMLM. The Nb/La ratio (0.31–0.56) of the samples also mostly belonged to the lithospheric mantle, and only a small amount belonged to the lithosphere–asthenosphere interaction field (>0.5, Smith et al., 1999). The Xishan basalts were plotted in the field between the within-plate and volcanic arc basalts (Figures 10C, D). Therefore, we believe that it was likely formed in the tectonic background of the transformation from the subduction environment to the plate internal environment.

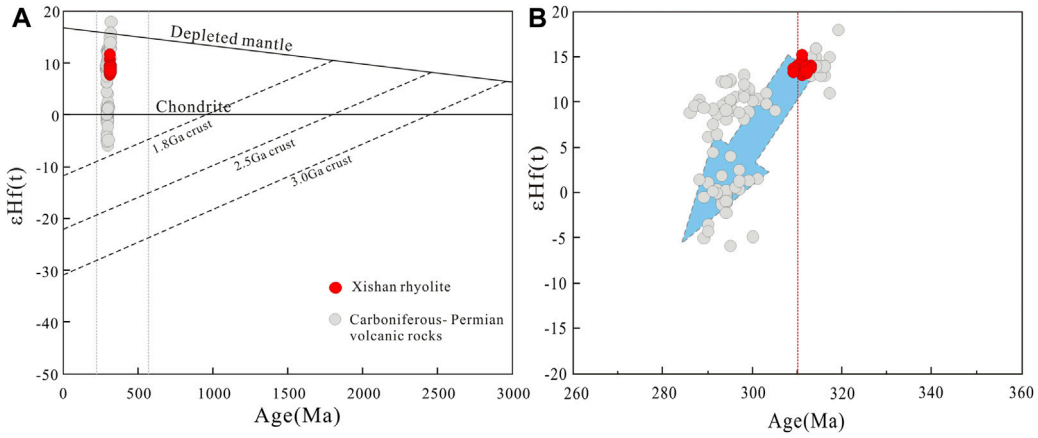

FIGURE 8
(A, B) Diagrams showing εHf (t) values vs. ages (Ma). The data for the Carboniferous-Permian volcanics are obtained from Chen et al. (2011) and Gao et al. (2014).

6.2.2 Petrogenesis of the andesites

Andesite showed moderate SiO_2, Al_2O_3, high TFe_2O_3, low P_2O_5, and Mg# contents, suggesting that it was not a primary mantle melt in equilibrium with mantle peridotite. The Late Carboniferous volcanic rock assemblage in the study area was basalt–andesite–rhyolite, which was close in time and space to the Dashitou basaltic–rhyolitic assemblage formation in the northwest of the study area (Zhang et al., 2017). The andesite genesis was either homogenous, that is, formed by the crystallization differentiation of basaltic magma or by mixing basaltic and rhyolitic magma. The lack of basaltic inclusions in andesites suggested that the magma mixing of the mantle- and crust-derivative melts was not a reasonable explanation. This was also supported by geochemical signatures. Both of these had SiO_2 and oxide correlations consistent with basalts, suggesting that some degree of crystallization differentiation may have occurred during the evolution of the associated primitive magmas, consistent with the bimodal volcanic suites. Andesites also generally have high La/Sm ratios (3.56–6.03), similar to the mantle-derived magmas that suffered from crustal materials (>5). Taken together, we suggest that andesites are the product of related melts that underwent assimilation mixing and crystallization differentiation.

6.2.3 Petrogenesis of the rhyolites

The Xishan rhyolites showed low MgO and CaO, as well as high SiO_2 and total alkali contents. Further, they were enriched with Zr, Nb, and Y contents and depleted with Ba, Sr, P, Ti, and Eu negative anomalies. Discrimination diagrams in Figure 11 are often used to explain the felsic intrusive rocks, but had also been used by some researchers to discuss the genetic type and tectonic environment of rhyolites (Chen et al., 2011; Zhang et al., 2017) due to the granites and rhyolites have the same magmatic source region and diagenetic tectonic environment. As seen from the discrimination diagrams (Figures 11A, B; Whalen et al., 1987), the abovementioned features indicated that the Xishan rhyolites are akin to A-type granites. In addition, they were closer to the tectonic environment of A_2-type granites (Figure 11C) and had comparatively low Nb/Y ratios (0.25–0.32) (Eby, 1992). The genesis of acidic magmas with an A-type affinity is controversial, including the crystallization differentiation of contemporaneous basaltic magmas (Peccerillo et al., 2003), mixing between the mantle-derived basalts and crustal-derived acidic magmas (Zhang et al., 2008), and partial melting of pre-existing crustal rocks (Tamura and Tatsumi, 2002). The basaltic–andesite–rhyolite samples showed good linearity for TiO_2, Al_2O_3, TFeO, MgO, CaO, and CaO/Al_2O_3 with SiO_2 in the variation charts (Figure 9). The Hf isotopes of the rhyolites ranged from 8.0 to 11.9, similar to basalts (Chen et al., 2011; Wali et al., 2018). This indicates that rhyolites may have been produced by the crystallization differentiation of basalts. Additionally, the rhyolite in the bimodal volcanic suite of Qijiaojing and Hongshankou is confirmed to be derived from the crystallization differentiation of basic rocks (Chen et al., 2013). The Xishan rhyolite samples were plotted in the field between the volcanic arc granitoids and within-plate granitoids (Figure 11D), which was most likely due to the tectonic environment transitioning from an island arc to an intraplate environment.

6.3 Tectonic implications

During the Carboniferous–Permian periods, the tectonic evolution of the BOB and Tianshan Orogenic Belt continued to be a matter of controversy. The primary viewpoints for this are as follows: 1) the tectonic setting for the transition from the Carboniferous subduction setting to the Permian post-collisional setting (Xiao et al., 2004a; Shu et al., 2011; Xie et al., 2016); 2) the post-collisional orogenic belt after the closing of the Tianshan Ocean at the end of the Early Carboniferous (Han et al., 2010; Chen et al., 2011); and 3) the Carboniferous–Permian continental rifting environment was related to the mantle plume (Gu et al., 2000; Xia et al., 2012).

Based on the combination of new research data and previous studies, it was confirmed that the majority of volcanics were formed in a back-arc tectonic setting during the early Late Carboniferous (Figures 6–8). Consequently, we eliminated the first scenario involving a post-collisional orogenic belt in the Tianshan Ocean

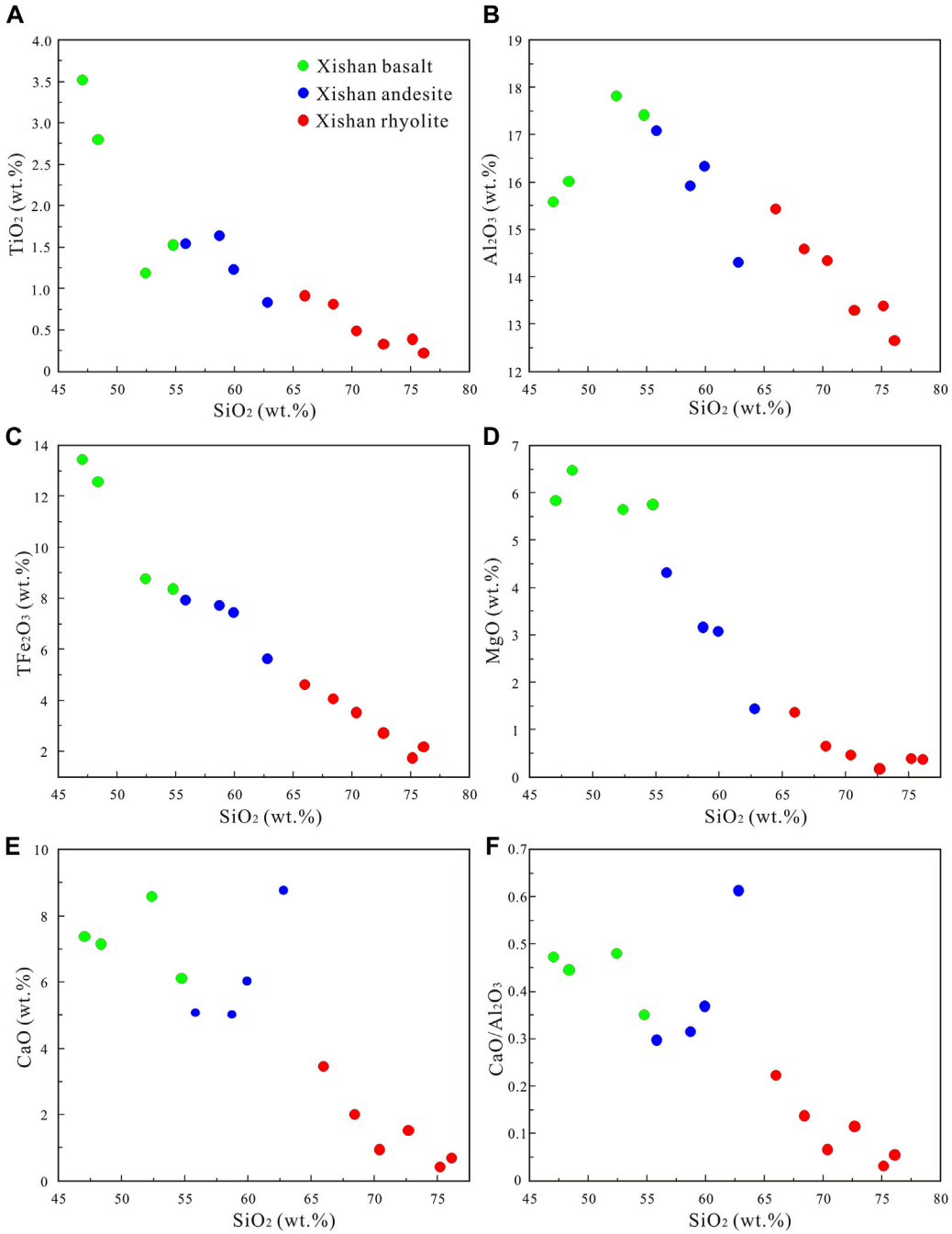

FIGURE 9
(A-F) Variation charts of major elements vs. SiO_2 for the volcanics in the Eastern BOB.

after closure toward the end of the Early Carboniferous. Note that the geochemical features of the Xishan basalts are distinctly different from those of the basaltic magmas produced by the mantle plumes. For instance, they have low LREE content and negative anomalies for Ti, Ta, and Nb. Our zircon saturation temperature (T_{Zr} = 814°C–871°C), which is calculated by adopting a typical approach (Watson and Harrison, 1983), for the Xishan rhyolites is substantially lower than that of the A-type granites associated with the Emeishan mantle plume (T_{Zr} = 934°C–1053°C, Xu et al., 2001) and A-type rhyolites prevalent in the Tarim LIP (T_{Zr} = 872°C–940°C, Liu et al., 2014). Apparently, the formation of the Xishan volcanics may not be related to the mantle plume. We have previously discussed the Xishan basaltic andesites and their characteristics. They display arc and intraplate basalt affinities, indicating a possible formation in a back-arc tectonic setting. The Xishan rhyolites also share some similarities with the tectonic environment of A_2-type granites (Figure 11C), suggesting an extensional setting. This is also supported by the Hf isotopes. εHf(t) values is positively correlated with age from 330 Ma to 290 Ma, representing the extensional setting (Figure 8B). After considering these conclusions, we

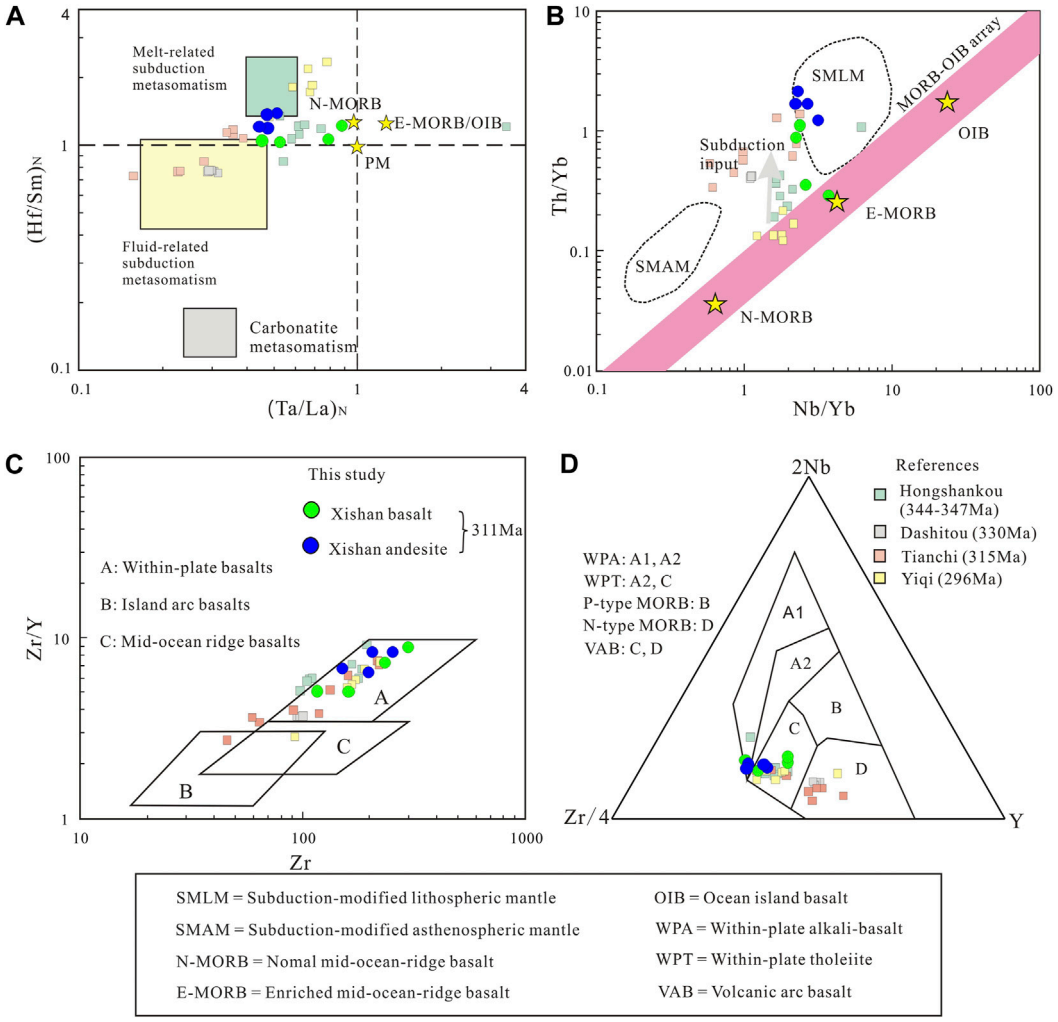

FIGURE 10
Source region discrimination diagrams for the volcanics in the eastern BOB. **(A)** After Flèche et al. (1998); **(B)** after Pearce (2008); **(C)** after Pearce and Norry (1979); **(D)** after Meschede (1986). The compositions of OIB, N-MORB, and E-MORB are obtained from Sun and McDonough (1989). Data sources are the same as in Figure 6.

propose herein that the tectonic evolution of the BOB and the entire Tianshan Orogenic Belt region occurred during the transition from an island arc magmatic system to a post-collisional orogenic belt. However, this study is of the opinion that this transition began toward the end of the Late Carboniferous.

The observed spatial and temporal variations and heterogeneity in the material origin of the Carboniferous–Permian magmatism in the BOB indicated that volcanics have multiple origins and genesis. Different bimodal volcanics are apparent not only in the western section of Bogda but also in its eastern section (Wang et al., 2010). This could be attributed to the magmatism differences during the different evolutionary stages. The prevalent belief is that the formation of the Bogda–Hallik Island Arc Belt occurred during the southward subduction of the Devonian–Carboniferous oceanic slab (Xiao et al., 2004b; Yuan et al., 2010). For instance, ophiolitic mélanges, such as Kelameili and Baiyanggou, which were discovered around the BOB (Qin et al., 2002; Chen et al., 2013; Xu et al., 2013), may be remnants of the Tianshan Ocean (Xiao et al., 2004b; Han et al., 2010). The Tianshan Ocean gradually subducted southward during the Late Devonian–Early Carboniferous periods. The BOB volcanism reached its peak during the Carboniferous and Permian periods.

Based on reliable chronological evidence, the bimodal volcanic activity in the Eastern Tianshan occurred during the Early Carboniferous to Early Permian periods (Wang et al., 2006; Shu et al., 2011; Chen et al., 2013). During the Early Carboniferous, a subducting plate rollback may have occurred at the north of the North Tianshan Island Arc, which led to gradual landward angulation, regional and transient extension, and the creation of bimodal volcanics with high-alumina basalts (Chen et al., 2013; Zhang et al., 2017). At the end of the Early Carboniferous, the closure of the Paleo-Tianshan Ocean and subsequent entry into a post-collisional orogenic setting (Han et al., 2010; Chen et al., 2011), marked a shift from extrusion to the extension of the geodynamic environment, which led to the formation of our current Xishan volcanic group (Figure 12). Toward the end of the Carboniferous period and the beginning of the Permian period, the Tianshan Ocean underwent

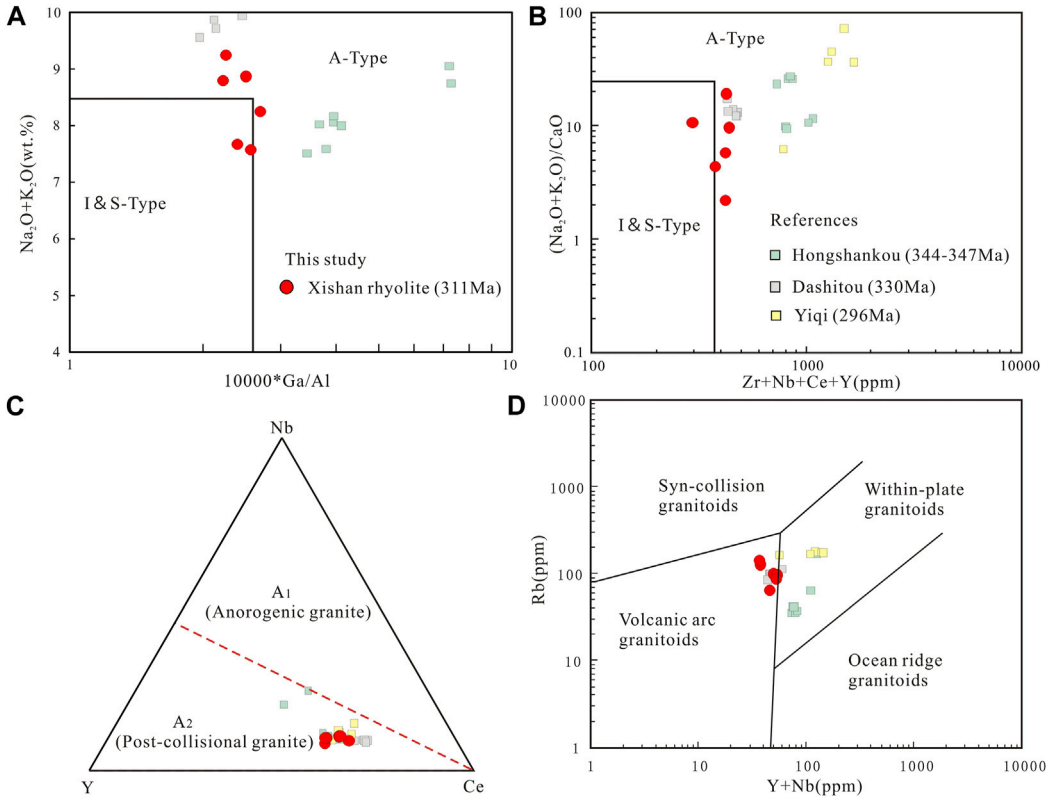

FIGURE 11
(A) and **(B)**: Discrimination diagrams of rock genetic type (after Whalen et al., 1987); **(C)** Nb–Y–Ce diagram (after Eby, 1992); **(D)** Rb vs. Y + Nb (after Pearce et al., 1984). Data sources are the same as in Figure 6.

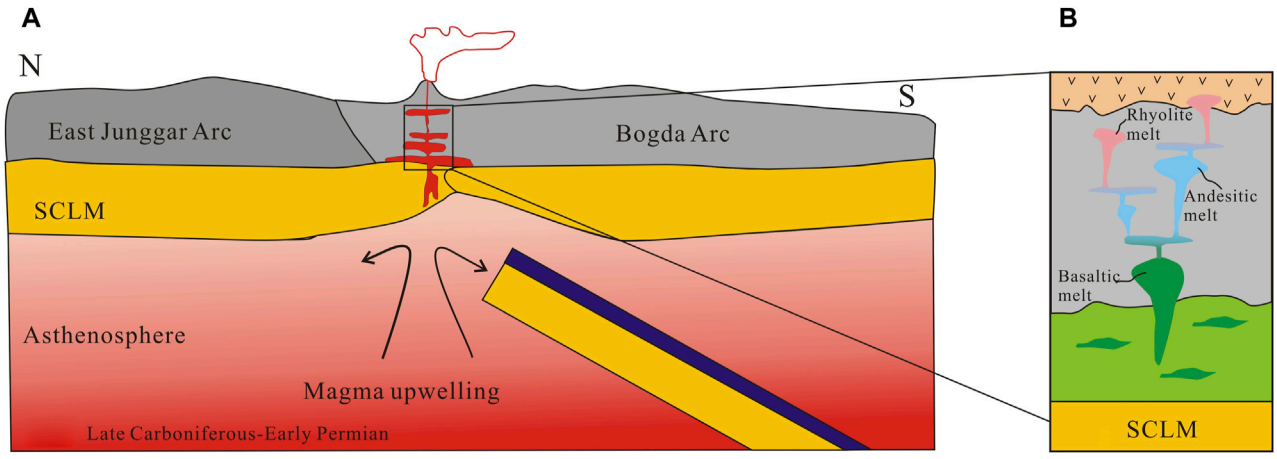

FIGURE 12
(A) Tectonic evolution modal of the BOB; **(B)** Schematic of the vertical section of the Xishan volcanics.

subduction and depletion. Extensive bimodal volcanics and basaltic dike swarm were formed in the early Permian period as a result of the post-collisional effects following the collision between the northern margins of the Siberian and Tarim continents (Chen et al., 2011; Xie et al., 2016; Wali et al., 2018) (Figure 12). The thick, coarse clastic rocks from the Late Permian subsequently evolved into a mud-sandstone sequence with rhythmic characteristics and stable clastic rock sedimentation of the Triassic. No further large-scale volcanic activity was observed. This denoted the actual end of the BOB magmatism and the onset of the quasi-plain stage for the entire region.

7 Conclusion

The following conclusions were derived from this work.

(1) Both the Liudaogou and Qidaogou sections in the eastern BOB belonged to the Upper Carboniferous Liushugou Formation (C_2l), which comprised continuous volcanic and sedimentary sequences.
(2) The Xishan volcanics comprised basalt, andesite, and rhyolite. Among them, rhyolites had zircon U–Pb ages of 311.2 ± 1.7 Ma, which, combined with the guide fossils *Plerophyllum* sp., *Zaphrentoides* sp., and *Zaphrentites* sp., indicate its formation to be in the Late Carboniferous.
(3) Basaltic rocks were derived from a metasomatized SCLM. Andesite and rhyolite were produced by crystallization differentiation of the basaltic rocks and assimilation mixing.
(4) The tectonic evolution of the transition from island arc magmatic systems to post-collisional orogenic belt in the BOB commenced at the end of the Late Carboniferous.

Data availability statement

The original contributions presented in the study are included in the article/Supplementary Material, further inquiries can be directed to the corresponding author.

Author contributions

W-JW: Data curation, Formal analysis, Investigation, Writing–original draft. Y-LH: Conceptualization, Data curation, Formal analysis, Investigation, Writing–review and editing. LX: Investigation, Writing–review and editing. W-BX: Writing–review and editing. W-XR: Data curation, Investigation, Writing–review and editing. H-TW: Investigation, Rock-mineral determination, Writing–review and editing. All authors contributed to the article and approved the submitted version.

Funding

This work was supported by the Natural Science Foundation of Sichuan Province (No. 2022NSFSC1734); the Doctoral Research Initiation Program of China West Normal University (No. 18Q018); and Xinjiang Geological Survey Program (No. T15-1-LQ20).

Acknowledgments

We thank researcher Wei-Hua Liao of the Nanjing Institute of Geology and Paleontology, Chinese Academy of Sciences, for his help in identifying fossils. We appreciate the kind help of Yi-Hu Zhang for LA–ICP–MS zircon dating. We thank Prof. Xi-Jun Liu and three reviewers for their constructive comments and language polishing of our manuscript.

Conflict of interest

The authors declare that the research was conducted in the absence of any commercial or financial relationships that could be construed as a potential conflict of interest.

Publisher's note

All claims expressed in this article are solely those of the authors and do not necessarily represent those of their affiliated organizations, or those of the publisher, the editors and the reviewers. Any product that may be evaluated in this article, or claim that may be made by its manufacturer, is not guaranteed or endorsed by the publisher.

Supplementary material

The Supplementary Material for this article can be found online at: https://www.frontiersin.org/articles/10.3389/feart.2023.1251107/full#supplementary-material

References

Ao, S., Xiao, W., Windley, B. F., Mao, Q., Han, C., Zhang, J. e., et al. (2016). Paleozoic accretionary orogenesis in the eastern beishan orogen: constraints from zircon U–Pb and $^{40}Ar/^{39}Ar$ geochronology. *Gondwana Res.* 30, 224–235. doi:10.1016/j.gr.2015.03.004

Aydin, F., Schmitt, A. K., Siebel, W., Sönmez, M., Ersoy, Y., Lermi, A., et al. (2014). Quaternary bimodal volcanism in the niğde volcanic complex (cappadocia, central anatolia, Turkey): age, petrogenesis and geodynamic implications. *Contributions Mineralogy Petrology* 168 (5), 1078. doi:10.1007/s00410-014-1078-3

Charvet, J., Liangshu, S., and Laurent-Charvet, S. (2007). Paleozoic structural and geodynamic evolution of eastern tianshan (NW China): welding of the Tarim and junggar plates. *Episodes* 30, 162–186.

Chen, X., Shu, L., and Santosh, M. (2011). Late paleozoic post-collisional magmatism in the eastern tianshan belt, northwest China: new insights from geochemistry, geochronology and petrology of bimodal volcanic rocks. *Lithos* 127 (3), 581–598. doi:10.1016/j.lithos.2011.06.008

Chen, X., Shu, L., Santosh, M., and Zhao, X. (2013). Island arc-Type bimodal magmatism in the eastern tianshan belt, northwest China: geochemistry, zircon U–Pb geochronology and implications for the paleozoic crustal evolution in central asia. *Lithos* 168-169, 48–66. doi:10.1016/j.lithos.2012.10.006

Eby, G. N. (1992). Chemical subdivision of the A-type granitoids:Petrogenetic and tectonic implications. *Geology* 20 (7), 641. doi:10.1130/0091-7613(1992)020<0641:CSOTAT>2.3.CO;2

Flèche, M. R. L., Camiré, G., and Jenner, G. A. (1998). Geochemistry of post-acadian, carboniferous continental intraplate basalts from the maritimes basin, magdalen islands, québec, Canada. *Chem. Geol.* 148 (3), 115–136. doi:10.1016/S0009-2541(98)00002-3

Frey, F. A., Green, D. H., and Roy, S. D. (1978). Integrated models of basalt petrogenesis: a study of quartz tholeiites to olivine melilitites from South eastern Australia utilizing geochemical and experimental petrological data. *J. Petrology* 19, 463–513. doi:10.1093/petrology/19.3.463

Gao, J., Li, W., Liu, J., Gao, Y., Guo, X., Zhou, Y., et al. (2014). Geochemistry, zircon U-Pb age and Hf isotopes of Late Carboniferous rift volcanic in the Sepikou region, eastern Bogda, Xinjiang. *Acta Petrol. Sin.* 30, 3539–3552. (in Chinese with English abstract).

Glorie, S., De Grave, J., Buslov, M. M., Zhimulev, F. I., Izmer, A., Vandoorne, W., et al. (2011). Formation and palaeozoic evolution of the gorny-altai–altai-Mongolia suture zone (South siberia): zircon U/Pb constraints on the igneous record. *Gondwana Res.* 20 (2), 465–484. doi:10.1016/j.gr.2011.03.003

Gu, L., Hu, S. X., and Wu, C. (2000). Carboniferous volcanites in the Bogda orogenic belt of eastern tianshan: their tectonic implications. *Acta Petrol. Sin.* 16, 305–316. (in Chinese with English abstract).

Han, B. F., Guo, Z. J., Zhang, Z. C., Zhang, L., Chen, J. F., and Song, B. (2010). Age, geochemistry, and tectonic implications of a late Paleozoic stitching pluton in the North Tian Shan suture zone, western China. *GSA Bull.* 122 (3-4), 627–640. doi:10.1130/B26491.1

Harley, S. L., and Kelly, N. M. (2007). The impact of zircon–garnet REE distribution data on the interpretation of zircon U–Pb ages in complex high-grade terrains: an example from the rauer islands, east Antarctica. *Chem. Geol.* 241 (1), 62–87. doi:10.1016/j.chemgeo.2007.02.011

He, G. Q., Li, M. S., Liu, D. Q., and Zhou, N. H. (1994). *Palaeozoic crustal evolution and mineralization in Xinjiang of China*. Urumqi: Xinjiang People's Publication House, 437.

Hofmann, A. W. (1997). Mantle geochemistry: the message from oceanic volcanism. *Nature* 385, 219–229. doi:10.1038/385219a0

Irvine, T. N., and Baragar, W. R. A. (1971). A guide to the chemical classification of the common volcanic rocks. *Can. J. Earth Sci.* 8 (5), 523–548. doi:10.1139/e71-055

Jackson, S. E., Pearson, N. J., Griffin, W. L., and Belousova, E. A. (2004). The application of laser ablation-inductively coupled plasma-mass spectrometry to *in situ* U–Pb zircon geochronology. *Chem. Geol.* 211 (1), 47–69. doi:10.1016/j.chemgeo.2004.06.017

Jahn, B. M., Wu, F. Y., and Chen, B. (2000). Massive granitoid generation in central asia: nd isotope evidence and implication for continental growth in the phanerozoic. *Episodes* 23 (2), 82–92. doi:10.18814/epiiugs/2000/v23i2/001

Kröner, A., Kovach, V., Belousova, E., Hegner, E., Armstrong, R., Dolgopolova, A., et al. (2014). Reassessment of continental growth during the accretionary history of the central asian orogenic belt. *Gondwana Res.* 25 (1), 103–125. doi:10.1016/j.gr.2012.12.023

Liu, H. Q., Xu, Y. G., Tian, W., Zhong, Y. T., Mundil, R., Li, X. H., et al. (2014). Origin of two types of rhyolites in the Tarim large igneous Province: consequences of incubation and melting of a mantle plume. *Lithos* 204, 59–72. doi:10.1016/j.lithos.2014.02.007

Liu, X. J., Zhang, Z. G., Xu, J. F., Xiao, W. J., Shi, Y., Gong, X. H., et al. (2020). The youngest permian ocean in central asian orogenic belt: evidence from geochronology and geochemistry of bingdaban ophiolitic mélange in central tianshan, northwestern China. *Geol. J.* 55 (3), 2062–2079. doi:10.1002/gj.3698

Long, X., Yuan, C., Sun, M., Safonova, I., Xiao, W., and Wang, Y. (2012). Geochemistry and U–Pb detrital zircon dating of paleozoic graywackes in east junggar, NW China: insights into subduction–accretion processes in the southern central asian orogenic belt. *Gondwana Res.* 21 (2), 637–653. doi:10.1016/j.gr.2011.05.015

Maniar, P. D., and Piccoli, P. M. (1989). Tectonic discrimination of granitoids. *Geol. Soc. Am. Bull.* 101 (5), 635–643. doi:10.1130/0016-7606(1989)101<0635:TDOG>2.3.CO;2

Mao, Q. G., Xiao, W. J., Wang, H., Ao, S. J., Windley, B. F., Song, D. F., et al. (2022). Prolonged late mesoproterozoic to late triassic tectonic evolution of the major Paleo-Asian Ocean in the beishan orogen (NW China) in the southern altaids. *Front. Earth Sci.* 9. doi:10.3389/feart.2021.825852

Meschede, M. (1986). A method of discriminating between different types of mid-ocean ridge basalts and continental tholeiites with the ocean ridge basalts and continental tholeiites with the Nb-Zr-Y diagram. diagram. *Chem. Geol.* 56 (3), 207–218. doi:10.1016/0009-2541(86)90004-5

Middlemost, E. (1994). Naming materials in the magma/igneous rock system. *Earth-Science Rev.* 37 (3-4), 215–224. doi:10.1016/0012-8252(94)90029-9

Pearce, J. A., and Norry, M. J. (1979). Petrogenetic implications of Ti, Zr, Y, and Nb variations in volcanic rocks. *Contributions Mineralogy Petrology* 69 (1), 33–47. doi:10.1007/BF00375192

Pearce, J. A. (2008). Geochemical fingerprinting of oceanic basalts with applications to ophiolite classification and the search for Archean oceanic crust. *Lithos* 100 (1-4), 14–48. doi:10.1016/j.lithos.2007.06.016

Pearce, J., Harris, N., and Tindle, A. (1984). Trace element discrimination diagrams for the tectonic interpretation of granitic rocks. *J. Petrology* 25, 956–983. doi:10.1093/petrology/25.4.956

Peccerillo, A., Barberio, M. R., Yirgu, G., Ayalew, D., Barbieri, M., and Wu, T. W. (2003). Relationships between mafic and peralkaline silicic magmatism in continental rift settings: a petrological, geochemical and isotopic study of the gedemsa volcano, central Ethiopian rift. *J. Petrology* 44 (11), 2003–2032. doi:10.1093/petrology/egg068

Peppe, D., and Deino, A. L. (2013). Dating rocks and fossils using geologic methods. *Nat. Educ. Knowl.* 4.

Pin, C., and Paquette, J. L. (1997). A mantle-derived bimodal suite in the hercynian belt: nd isotope and trace element evidence for a subduction-related rift origin of the late devonian Brévenne metavolcanics, massif central (France). *Contributions Mineralogy Petrology* 129 (2), 222–238. doi:10.1007/s004100050334

Qin, K., Sun, S., Li, J., Fang, T., Wang, S., and Liu, W. (2002). Paleozoic epithermal Au and porphyry Cu deposits in north Xinjiang, China: epochs, features, tectonic linkage and exploration significance. *Resour. Geol.* 52 (4), 291–300. doi:10.1111/j.1751-3928.2002.tb00140.x

Sengör, A. M. C., Natal'In, B. A., and Burtman, V. S. (1993). Evolution of the Altaid tectonic collage and Palaeozoic crustal growth in Eurasia. *Nature* 364, 299–307. doi:10.1038/364299a0

Shinjo, R., and Kato, Y. (2000). Geochemical constraints on the origin of bimodal magmatism at the Okinawa Trough, an incipient back-arc basin. *Lithos* 54 (3), 117–137. doi:10.1016/S0024-4937(00)00034-7

Shu, L. S., Deng, X. L., Zhu, W. B., Ma, D. S., and Xiao, W. J. (2011). Precambrian tectonic evolution of the Tarim block, NW China: new geochronological insights from the quruqtagh domain. *J. Asian Earth Sci.* 42 (5), 774–790. doi:10.1016/j.jseaes.2010.08.018

Shu, L., Wang, B., Zhu, W., Guo, Z., Charvet, J., and Zhang, Y. (2011). Timing of initiation of extension in the Tianshan, based on structural, geochemical and geochronological analyses of bimodal volcanism and olistostrome in the Bogda Shan (NW China). *Int. J. Earth Sci.* 100 (7), 1647–1663. doi:10.1007/s00531-010-0575-5

Sun, S. S., and McDonough, W. F. (1989). Chemical and isotopic systematics of oceanic basalts: implications for mantle composition and processes. *Geol. Soc. Lond. Spec. Publ.* 42 (1), 313–345. doi:10.1144/GSL.SP.1989.042.01.19

Sun, M., Yuan, C., Xiao, W., Long, X., Xia, X., Zhao, G., et al. (2008). Zircon U–Pb and Hf isotopic study of gneissic rocks from the Chinese altai: progressive accretionary history in the early to middle palaeozoic. *Chem. Geol.* 247 (3), 352–383. doi:10.1016/j.chemgeo.2007.10.026

Tamura, Y., and Tatsumi, Y. (2002). Remelting of an andesitic crust as a possible origin for rhyolitic magma in oceanic arcs: an example from the izu–bonin arc. *J. Petrology* 43 (6), 1029–1047. doi:10.1093/petrology/43.6.1029

Tan, J. Y., Wang, S. F., Wu, R. J., Zhang, Y., and Guo, Z. (2010). Types and time of Carboniferous volcanic edifices in eastern Junggar, Xinjiang. *Acta Petrol. Sin.* 26, 440–448. (in Chinese with English abstract).

Wali, G., Wang, B., Cluzel, D., and Zhong, L. (2018). Carboniferous – early permian magmatic evolution of the Bogda range (Xinjiang, NW China): implications for the late paleozoic accretionary tectonics of the SW central asian orogenic belt. *J. Asian Earth Sci.* 153, 238–251. doi:10.1016/j.jseaes.2017.07.045

Wang, B., Chen, Y., Zhan, S., Shu, L., Faure, M., Cluzel, D., et al. (2007). Primary carboniferous and permian paleomagnetic results from the yili block (NW China) and their implications on the geodynamic evolution of Chinese tianshan belt. *Earth Planet. Sci. Lett.* 263 (3), 288–308. doi:10.1016/j.epsl.2007.08.037

Wang, B., Shu, L., Faure, M., Jahn, B. M., Cluzel, D., Charvet, J., et al. (2011). Paleozoic tectonics of the southern Chinese tianshan: insights from structural, chronological and geochemical studies of the heiyingshan ophiolitic mélange (NW China). *Tectonophysics* 497 (1), 85–104. doi:10.1016/j.tecto.2010.11.004

Wang, J., Taide, L. I., Tian, L., Man, Y. U., Wang, H., Zhao, Z. A., et al. (2010). Co-Occurrence of victimization from five subtypes of bullying: physical, verbal, social exclusion, spreading rumors, and cyber. *Acta Petrol. Sin.* 26, 1103–1112. (in Chinese with English abstract). doi:10.1093/jpepsy/jsq048

Wang, W. J., Li, X. W., Chen, W. F., Qiu, L., Zhang, Y. H., and Zhao, Z. X. (2023). Basement differences control granitoid compositions: insights from zircon Hf isotopic mapping of paleozoic granitoids in the northern beishan orogenic collage, NW China. *Int. Geol. Rev.*, 1–27. doi:10.1080/00206814.2023.2246063

Wang, X. W., Xu, X. Y., Ma, Z. P., Chen, J. L., Zhu, X. H., Sun, J. M., et al. (2015). Geochemical characteristics of the Late Carboniferous bimodal volcanic rocks in Jijitaizi area, eastern Bogda orogenic belt, and their geological significance. *Geol. China* 42 (3), 553–569. (in Chinese with English abstract). doi:10.12029/gc20150312

Wang, Y., Gu, L., Zhang, Z., Wu, C., Zhang, K. J., Li, H., et al. (2006). Geochronolgy and Nd-Sr-Pb isotopes of the bimodal volcanic rocks of the Bogda rift. *Acta Petrol. Sin.* 22, 1215–1216. (in Chinese with English abstract).

Wang, Y. X., Go, L. X., Zhang, Z. Z., Wu, C. Z., and Yang, J. D. (2006). Geochronology and Nd-Sr-Pb isotops of the bimodal volcanic rocks of the Bogda rift. *Acta Petrol. Sin.* 22 (5), 1215–1224. (in Chinese with English abstract).

Wartes, M. A., Carroll, A. R., and Greene, T. J. (2002). Permian sedimentary record of the turpan-hami basin and adjacent regions, northwest China: constraints on postamalgamation tectonic evolution. *GSA Bull.* 114 (2), 131–152. doi:10.1130/0016-7606(2002)114<0131:PSROTT>2.0.CO;2

Watson, E. B., and Harrison, T. M. (1983). Zircon saturation revisited: temperature and composition effects in a variety of crustal magma types. *Earth Planet. Sci. Lett.* 64 (2), 295–304. doi:10.1016/0012-821X(83)90211-X

Whalen, J. B., Currie, K. L., and Chappell, B. W. (1987). A-Type granites: geochemical characteristics, discrimination and petrogenesis. *Contributions Mineralogy Petrology* 95 (4), 407–419. doi:10.1007/BF00402202

Windley, B. F., Alexeiev, D., Xiao, W., Kröner, A., and Badarch, G. (2007). Tectonic models for accretion of the central asian orogenic belt. *J. Geol. Soc.* 164 (1), 31–47. doi:10.1144/0016-76492006-022

Xia, L. Q., Xu, X. Y., Xia, Z. C., Li, X. M., Ma, Z. P., and Wang, L. S. (2004). Petrogenesis of Carboniferous rift-related volcanic rocks in the Tianshan, northwestern China. *GSA Bull.* 116 (3-4), 419–433. doi:10.1130/B25243.1

Xia, L., Xu, X., Li, X., Ma, Z., and Xia, Z. (2012). Reassessment of petrogenesis of Carboniferous–Early Permian rift-related volcanic rocks in the Chinese Tianshan and its neighboring areas. *Geosci. Front.* 3 (4), 445–471. doi:10.1016/j.gsf.2011.12.011

Xiao, W. J., Mao, Q. G., Windley, B. F., Han, C. M., Qu, J. F., Zhang, J. E., et al. (2010). Paleozoic multiple accretionary and collisional processes of the Beishan orogenic collage. *Am. J. Sci.* 310 (10), 1553–1594. doi:10.2475/10.2010.12

Xiao, W., Windley, B. F., Badarch, G., Sun, S., Li, J., Qin, K., et al. (2004a). Palaeozoic accretionary and convergent tectonics of the southern altaids: implications for the growth of central asia. *J. Geol. Soc.* 161 (3), 339–342. doi:10.1144/0016-764903-165

Xiao, W., Windley, B. F., Han, C., Liu, W., Wan, B., Zhang, J. e., et al. (2018). Late Paleozoic to early Triassic multiple roll-back and oroclinal bending of the Mongolia collage in Central Asia. *Earth-Science Rev.* 186, 94–128. doi:10.1016/j.earscirev.2017.09.020

Xiao, W., Zhang, L. C., Qin, K. Z., Sun, S., and Li, J. L. (2004b). Paleozoic accretionary and collisional tectonics of the eastern tianshan (China): implications for the continental growth of central asia. *Am. J. Sci. - AMER J SCI* 304, 370–395. doi:10.2475/ajs.304.4.370

Xie, W., Xu, Y. G., Luo, Z. Y., Liu, H. Q., Hong, L. B., and Ma, L. (2016). Petrogenesis and geodynamic implications of the late carboniferous felsic volcanics in the Bogda belt, Chinese northern tianshan. *Gondwana Res.* 39, 165–179. doi:10.1016/j.gr.2016.07.005

Xu, Q. Q., Ji, J. Q., Zhao, L., Gong, J. F., Zhou, J., He, G. Q., et al. (2013). Tectonic evolution and continental crust growth of northern Xinjiang in northwestern China: remnant ocean model. *Earth-Science Rev.* 126, 178–205. doi:10.1016/j.earscirev.2013.08.005

Xu, Y., Chung, S. L., Jahn, B. M., and Wu, G. (2001). Petrologic and geochemical constraints on the petrogenesis of Permian–Triassic Emeishan flood basalts in southwestern China. *Lithos* 58 (3), 145–168. doi:10.1016/S0024-4937(01)00055-X

Yang, Y. Q., Zhao, L., Zhang, J., and Niu, M. L. (2021). Middle paleozoic archipelago amalgamation and tectonic transform in the northern west junggar, NW China: constraints from magmatism and deformation. *Gondwana Res.* 98, 147–165. doi:10.1016/j.gr.2021.04.010

Yang, Y. Q., Zhao, L., Zheng, R. G., Xu, Q. Q., Liu, J. H., and Zhang, J. (2020). An Early Ordovician fossil seamount of the Hongguleleng-Balkybey Ocean in the northern West Junggar terrane (NW China) and its implications for the ocean evolution. *J. Asian Earth Sci.* 194, 104066. doi:10.1016/j.jseaes.2019.104066

Yuan, C., Sun, M., Wilde, S., Xiao, W., Xu, Y., Long, X., et al. (2010). Post-collisional plutons in the balikun area, east Chinese tianshan: evolving magmatism in response to extension and slab break-off. *Lithos* 119 (3), 269–288. doi:10.1016/j.lithos.2010.07.004

Zhang, W., Hu, Z., and Spectroscopy, A. (2020). Estimation of isotopic reference values for pure materials and geological reference materials. *At. Spectrosc.* 41, 93–102. doi:10.46770/AS.2020.03.001

Zhang, X., Zhang, H., Tang, Y., Wilde, S. A., and Hu, Z. (2008). Geochemistry of permian bimodal volcanic rocks from central inner Mongolia, north China: implication for tectonic setting and phanerozoic continental growth in central asian orogenic belt. *Chem. Geol.* 249 (3), 262–281. doi:10.1016/j.chemgeo.2008.01.005

Zhang, Y. X., Zeng, Z. G., Gaetani, G., Zhang, L., and Lai, Z. Q. (2020). Mineralogical constraints on the magma mixing beneath the iheya graben, an active back-arc spreading centre of the okinawa trough. *J. Petrology* 61 (9). doi:10.1093/petrology/egaa098

Zhang, Y., Yuan, C., Long, X., Sun, M., Huang, Z., Du, L., et al. (2017). Carboniferous bimodal volcanic rocks in the eastern tianshan, NW China: evidence for arc rifting. *Gondwana Res.* 43, 92–106. doi:10.1016/j.gr.2016.02.004

Zong, K., Klemd, R., Yuan, Y., He, Z., Guo, J., Shi, X., et al. (2017). The assembly of rodinia: the correlation of early neoproterozoic (ca. 900Ma) high-grade metamorphism and continental arc formation in the southern beishan orogen, southern central asian orogenic belt (CAOB). *Precambrian Res.* 290, 32–48. doi:10.1016/j.precamres.2016.12.010